Modeling of the planetary ball-milling process: The case study of ceramic powders

M. Broseghini[a], L. Gelisio[a], M. D'Incau[a,*], C.L. Azanza Ricardo[a], N.M. Pugno[b,c,d], P. Scardi[a]

[a] *Department of Civil, Environmental & Mechanical Engineering, University of Trento, via Mesiano, 77, 38123 Trento, Italy*

[b] *Department of Civil, Environmental & Mechanical Engineering, Laboratory of Bio-Inspired and Graphene Nanomechanics, University of Trento, via Mesiano, 77, 38123 Trento, Italy*

[c] *Center for Materials and Microsystems, Fondazione Bruno Kessler, Via Sommarive 18, 38123 Povo (Trento), Italy*

[d] *School of Engineering and Materials Science, Queen Mary University of London, Mile End Road, London E1 4NS, United Kingdom*

[*] *Corresponding author: mirco.dincau@unitn.it.*

Abstract

A numerical dynamic-mechanical model of a planetary ball-mill is developed to study the dependence of process efficiency on milling parameters like ball size and number, jar geometry and velocity of the revolving parts. Simulations provide evidence of the correlation between milling parameters and the resulting microstructure ofthe ground material. In particular, maximum efficiency ofthe grinding process is observed with the most disordered ball motion, which is obtained within a well-defined range of jar to plate velocity ratios. As a significant case study in ceramic powder technology, the model is presented and validated for calcium fluoride (CaF2), ground under different conditions in a planetary mill, and then characterized by X-ray powder diffraction and scanning electron microscopy.

Keywords

Ball milling, Multibody simulations, X-ray diffraction, Microstructure, CaF2

1. Introduction

High-energy ball milling is commonly used for particle size reduction (comminution) down to the nanometer scale [6,16,62]. Increased surface energy and defectivity lead to modified physical/chemical properties and can promote structural transformations and/or chemical reactions (see e.g. [67]). Nearly all materials can be processed, including metals [12,50,59], organics [31,54,61] and pharmaceuticals [39,47,48], as well as composites [14,40] or low-dimensional structures [2,8,15,38,71]. Ceramic materials can be produced either (i) indirectly or (ii) directly [58] via ball milling. While the former route promotes enhanced reactivity of starting materials (due to morphological, structural and/or chemical modifications) [34] and/or their deagglomeration [50], therefore improving the consecutive thermal treatment, the latter results in the direct manufacture of the desired end-product [10,35,60,68]. This is usually nanostructured, characterized by a selected polymorph [19,69,70], and affected by defects which are exploited to tune selected properties [24,29]. Furthermore, ceramics can be incorporated into different matrices by ball milling, so to enhance mechanical properties [28].

Among high-energy ball mills, the planetary is a mechanically simple and versatile device for efficient grinding. It is usually made of two or more jars, rotating at an angular velocity ω around their axis (see Fig. 1), installed on a disk rotating at angular velocity. Grinding occurs by impact among the milling media (balls and jars), driven by centrifugal and Coriolis forces, with material particles typically covering balls and/or jar surfaces. The energy available for comminution and, in turn, the size of the

ground particles and their defectivity, are determined by several parameters, related both to geometry and to physical properties of jar and milling media. These include size and shape of balls and jar, elasto-plastic properties and friction coefficients, but also angular velocities, grinding time and charge fraction. Products homogeneity and contamination from the vials are also related to the above-defined parameters and must be properly accounted for. The (i) straightforward approach to correlate milling parameters to end products is running the mill under different conditions. The alternative to this brute-force, time consuming empirical approach is modeling the process, either (ii) analytically [1,5,51] or (iii) numerically [17,30,33,42,44,53]. The main advantage of modeling over experimental testing is a better control over kinematic and dynamic quantities, e.g. ball trajectories and kinetic energies, under all possible operating conditions. Analytical models are elegant and informative but, most often, limited by simplifying assumptions, like inelasticity of collisions or approximate friction models.Numerical multibody models, although more computationally demanding, can preserve the main complexity of the milling process and possibly provide more accurate predictions.

This work introduces a model belonging to the latter category, implemented within the framework of a multibody dynamics software. The validity of the model has been experimentally verified considering the case study of a typical ceramic material, calcium fluoride.

2. The model

Following, the model of the Fritsch Pulverisette 4 (P4 [18]) planetary ball mill is presented. The solution of the equation of motion of the milling media is obtained, implementing a suitable model for contacts and Lagrangian description, by the software MSC.Adams [45]. One of the most appealing features of this multibody dynamics software is the aptitude for handling complicated mechanical systems, therefore allowing a detailed description of different processing apparatuses. Due to its limited volume fraction, powder charge has not been explicitly modeled but accounted for by a suitable choice of collision contact parameters [17], as will be discussed later.

The Hilber–Hughes–Taylor (HHT [26,46]) integrator, with automatic step tuning, was adopted setting a maximum numerical error of 10−8.

2.1. The mill

The angular velocities ω and (see Fig. 1) were applied, respectively, to the two hinges (features predefined in the MSC.Adams software) connecting (i) the jar (radius RJ) to the main disk (radius RP = 125 mm) and (ii) the latter to the ground reference frame. Milling media were randomly placed inside the jar, in the gravitational field, and angular velocities were gradually increased to the target values during the first second of simulation, which lasted overall 24 s. To allow motion homogenization, the first 4 s were discarded during data analysis. Properties of jar and milling media are reported in Table 1.

2.2. Contact modeling

The most critical ingredient in the model of a ball mill is the contact law. Contact models belong either to the (i) discrete or (ii) continuous approach [20]. While (i)is based on momentum balances, in (ii) a force–displacement law is added to the equation of motion, as a combination of a spring in parallel with a damper, causing energy dissipation, plus a friction element. The most significant formulations are based on a combination of either linear or non-linear spring or damper but more complicated schemes, such as those based on Mindlin’s work or on the introduction of plasticity, have also been proposed [13,20,22,37,53].

The contact force is defined by the hard-coded impact function [45], based on the non-linear spring (Fk) and linear damper scheme (Fd) proposed by Dubowsky and Freudenstein (impact pair model [13]),

$$F_c = F_k + F_d = ku^n + c\dot{u}, \tag{1}$$

being u and u˙ the relative displacement and velocity of the colliding bodies, whereas k and c are the spring generalized stiffness and the damping coefficient. With respect to the above formulation, to prevent discontinuities, the impact function, defined within MSC.Adams, implements a damping coefficient which depends on the relative displacement of colliding bodies,

$$c = -c_m \left(\frac{u}{d}\right)^2 \left(3 - 2\frac{u}{d}\right), \tag{2}$$

and varies from zero to cm, assuming the latter value when the relative displacement is greater than or equal to d. With the exponent n = 3/2, an estimate of k can be derived from the Hertzian theory of contact [22],

$$k = \frac{4}{3\pi}\left(\frac{1}{\eta_i + \eta_j}\right)\sqrt{\frac{R_i R_j}{R_i + R_j}}, \tag{3}$$

for the contact between sphere i and j, with radius R, and

$$k = \frac{4}{3\pi}\left(\frac{1}{\eta_i + \eta_j}\right)\sqrt{R_i}, \tag{4}$$

for the contact between sphere i and a plane (approximating jar surface). The parameter i = (1 − 2 i)/(Ei) accounts for elastic properties of materials, being the Poisson ratio and E the Young modulus. The solution ofthe classical problem of damped vibration of a mass spring system provides a guess of maximum the damping parameter [13],

$$c_m = -2\ln(e)\sqrt{\frac{1}{\ln^2(e) + \pi^2}}\sqrt{m_e k^*}, \tag{5}$$

being e the restitution coefficient, accounting for the difference from initial (h0) and final (h) height in a drop test, 1/me = 1/mi + 1/mj and k* [11],

$$k^* = \left(\frac{320}{81} m_e \dot{u}_{n0}^2 E_e^4 R_e^2\right)^{1/5}. \tag{6}$$

Geometrical and elastic properties are expressed, respectively, as 1/Re = 1/Ri + 1/Rj and 1/Ee = 1/Ei + 1/Ej whereas u˙ n0 is the relative velocity during the collision, assumed to be an average value for the discussed model (Table 2).

While calculations provide a reasonable first-order guess, experiments can account for simplifying assumptions in theories. The most straightforward approach is comparing a simulation of a drop test (ball impinging on a plane) against experimental results [43,44], measuring the first rebound height (h) and fitting d. This implies that some spread in the damping parameter is introduced depending on the compenetration.

Even if more refined contact models exist, it is worth noting that physical insights can be captured also from simpler (but more robust) schemes. Dealing with more complicated descriptions of phenomena is conditioned to a rigorous and extended procedure of parameters fitting.

Among the possible schemes to account for friction at the contact location, the Coulomb model (hardcoded in MSC.Adams) was implemented. In this case, parameters are the static (s) and dynamic (d) friction coefficients (Table 3). Again, to avoid discontinuities MSC.Adams expresses the friction coefficient as a function of the slip velocity (v),

$$\mu = \begin{cases} \mu_s \left(\frac{v}{v_s}\right)^2 \left(3 - 2\frac{v}{v_s}\right) & 0 \le v < v_s \\ \mu_s - (\mu_s - \mu_d)\left(\frac{v - v_s}{v_d - v_s}\right)^2 \left(3 - 2\frac{v - v_s}{v_d - v_s}\right) & v_s \le v < v_d, \\ \mu_d & v \ge v_d \end{cases} \quad (7)$$

therefore gradually varying from the static to the dynamic values.

3. Results and discussion

Calcium fluoride (CaF2) was ground using the above-described mill under several operating conditions (reported in the following paragraph) and ball milling effect was indirectly assessed by a rigorous characterization of the processed material either by (i) scanning electron microscopy (SEM) and (ii) X-ray powder diffraction (XRPD) line profile analysis (LPA [65,66]). Concisely, the latter consists in extracting structural and microstructural information from the width and the shape of diffraction peaks through suitable models. XRPD data were therefore analyzed by the Whole Powder Pattern Modeling approach (WPPM,[55–57]), so to provide the distribution of crystalline domains (assumed to be spherical) sizes, in terms of average (D) and standard deviation of a lognormal size distribution, and dislocation density ( ), expected to increase as a result of the milling procedure [3,4,12,25,27,52,64]. The more the process is protracted in time, the more the average crystallite dimension decreases and the density of defects increases.

Interestingly, 1/ D is related to the yield stress (y) through Hall–Petch law [23,49] and √ is connected to the work-hardening through Taylor equation [63]: qualitatively, Fig. 2 illustrates the increasing in yield stress and work-hardening as a function of milling time.

3.1. Analysis of results

Computer simulations provide the complete set of dynamical variables for each milling body as well as quantities associated to each contact event, therefore allowing an outright understanding of the time evolution of the investigated system. Naturally, visual inspection of trajectories provides information on (i) motion regimes and (ii) regions characterized by high impact frequency and/or intensity, therefore potentially prone to significant wear. Moreover, each computed quantity can be broken down with respect to the local impact reference frame, therefore allowing to design the preferential direction for stress exchange. For example, exfoliation of graphite can be enhanced if shear load is preferentially transferred [2,15,36].

To quantitatively characterize each simulation, two parameters have beenused. First one,the total relative impact energy ofthe system, computed in the impact reference frame [22,32,33,41,42,53], provides an upper bound estimate of the maximum amount of energy available for grinding the mill charge [7]

$$\frac{E_I}{\tau} = \frac{1}{2\tau}\sum_{j=1}^{C} \frac{m_{1j}m_{2j}}{m_{1j} + m_{2j}} \dot{u}_j^2, \quad (8)$$

where mi is the mass of the i-th colliding body, C is the number of collisions during the time period and u˙ the relative velocity. The latter quantity, and in turn the specific energy, can be decomposed into a normal (u˙ n) and a tangential (u˙ t) component with respect to the impact reference frame.

The second parameter provides a geometrical view of the simulation. Inspired by statistical mechanics, given the number of milling media N and the jar volume V, the Cylindrical Distribution Function (CDF),

$$g(r) = \frac{1}{2\pi hr\Delta r}\frac{V}{N}\langle\sum_{i=1}^{N}\delta\left(\vec{r}_i\cdot\hat{r}-r\right)\rangle_\tau, \qquad (9)$$

expresses the time-averaged density of milling media as a function of the distance from the jar axis (r i · rˆ for the i-th body), i.e. the probability of a given cylindrical shell having width r of being occupied (ı (x) is the Dirac's delta function and indicates the time average over the period). For a cylindrical jar, the more the CDF is uniform across the radius, the more the motion is random and the mean free path is large. To condense the randomness of motion, i.e. the absence of strong localization of milling media, in a single parameter, the reciprocal of the variance of the CDF histogram (1/) has been evaluated: the more uniform is the g (r) the larger is 1/ whereas, the more localized is the motion the smaller is 1/ .

3.2. Simulations

Within the wide set of parameters characterizing the process, in this work the effect of jar (ω) and plate () velocities on milling efficiency has been investigated. Following the approach by Rosenkranz et al. [53], the mill feed was accounted for by modifying friction coefficients, s and d (see Table 3). The observation was derived from the analysis of camera images revealing the formation of powder coating layers on balls and jar surfaces, strongly modifying friction conditions. It is also worth noting that for the presented case the powder charge volume is much smaller than that of the milling chamber and balls (volume fraction < 1%), so that the powder layer should not substantially affect restitution and thus the damping coefficient. Therefore, two extreme conditions have been simulated, namely characterized by (i) steel–steel and (ii) steel–fluorite friction coefficients. Moreover, to maximize energy exchange, jar and plate were rotated counter-clockwise [41].

Fig. 3 shows the outcome of selected simulations (ω = −320, −600, −800 rpm and = 200 rpm), illustrating both trajectories and the CDF for different motion regimes. In the first column, abovementioned quantities are computed for a low jar velocity ω: as made apparent from the trajectories, motion is not random and space regions of higher occupancy are present. Consequently, the CDF is not uniform. With respect to the previous case, the motion described within the second column is more random, with trajectories across the whole jar (longest mean free path), so that the observed CDF is nearly uniform. The last case, corresponding to high jar velocity, as clearly shown by trajectories, is characterized by balls chiefly sticking to the jar surfaces and consequently probability of crossing some regions is far from being uniform.

The specific impact energy (Eq. (8)) for sets of simulations performed at different fixed value of plate angular velocity for the steel–steel interaction case is reported in Fig. 4a. Interestingly, the effect of this parameter only affects the total amount of kinetic impact energy involved in the process whereas it does not alter the location (in terms of ω/ + 1) of the maximum energy exchange (corresponding to the central column in Fig. 3), therefore suggesting that, for a specific set of coefficients (representing the interaction between two specific materials), it is the geometry of the system that determines the most efficient milling condition. Particularly, it exists a critical ratio of angular velocities (expressed as ω/ + 1) corresponding to the maximum energy transfer: with respect to Fig. 3, ball motion is disordered, with trajectories across the whole jar, below this threshold (cascading to cataracting regime), whereas, above it, balls tend to stick to the jar surfaces (rolling).

As anticipated, the specific impact energy can be separated into a normal and tangential component with respect to the local impact reference frame. Fig. 4b depicts Eq. (8) computed for the above-described set of simulations performed at = 200 rpm. The contribution of the tangential component is higher, but the two trends are qualitatively similar, with the maximum of energy exchange corresponding to the same ω/ + 1 abscissa of ≈2.6.

The geometrical parameter, quantifying the randomness of motion of the milling media inside the jar and, in turn, the mean free path, is reported in Fig. 5a. Again, the location of the maximum Fig. 5a. Again, the location of the maximum is shared across simulations with different plate angular velocities and its value does not show a significant dependency on . A comparison between the energetic and geometrical parameters is shown in Fig. 5b for the steel–steel interaction case at = 200 rpm: the qualitative agreement of the two demonstrates that the more random is the motion, the higher is the energy exchange.

So far, only the steel–steel interaction (no powder charge) has been considered. To validate the model, a comparison of simulations and experimental results, i.e. grinding of calcium fluorite, was performed. The effect of the presence of the ceramic powder in the milling system was taken into account by modifying the parameters of the friction contact model (see Table 3): Fig. 6 illustrates the comparison between the specific impact energy computed for simulations performed at = 200 rpm using both coefficients representing the no-feed (red) and the fluorite powder (grey) cases. As demonstrated in the plot, fluorite presence is responsible for a shift of the maximum energy exchange condition, from ω/ + 1 ≈ −2.6 to ≈−3.0, and an increasing amount of energy exchanged.

The same figure also reports some interesting experimental results for fluorite powder ball-milled in a P4 mill under the same nominal conditions as in the simulations. Experimental data, as provided by LPA of the XRPD patterns, are proposed in terms of average crystallite dimensions (sphere diameter) D , and dislocation density, . In particular the Hall–Petch trend (1/ D) and the Taylor trend (√), which are both relevant to plasticity and in general to the powder comminution features, are illustrated. Impact kinetic energy computed from simulations nicely maps the trend of the experiments, thus providing a further validation of the proposed approach to simulate the milling process.

4. Conclusions and further developments

In this work a computer model for the P4 planetary ball mill has been presented and the effect of plate and jar velocity investigated. Two extreme conditions have been simulated, namely (i) steel–steel interaction (no mill charge) and (ii) steel–fluorite, by changing friction coefficients. Both cases have been analyzed from energetic and geometrical points of view. Results show that these, described by the specific kinetic impact energy and motion randomness parameters, are strictly related. In particular, the maximum value of the two parameters has been found to correspond to the same speed ratio, ω/ + 1 (cataracting motion regime), clearly indicating that the more the motion is complex the higher is the energy available for grinding. Moreover, for each set of contact coefficients, representing one the two milling conditions analyzed, results point out that the increment of plate angular velocity , has an influence only on the amount of energy involved and not on the maximum location, suggesting that the geometry of the system dominates. The more efficient grinding condition was found to be at ω/ + 1 ≈ −2.6 for the case of steel–steel and at ω/ + 1 ≈ −3.0 for steel–fluorite interaction. The shift of the maximum is therefore due to the lowering of friction and indicates that, when fluorite is present, higher velocity ratios are required to achieve the most efficient grinding.

Simulation output were also indirectly compared with experimental data from XRPD-LPA of ground fluorite. Particularly, average crystallite size and dislocation density have been characterized and related to mechanical properties through Hall–Petch law (yield stress) and Taylor equation (work hardening). In spite of the simplicity of the model used to simulate contacts, a good agreement has

been found within the two extreme conditions. The choice of a straightforward contact scheme is due to the not trivial calculation and tuning of model coefficients, which are the key ingredient for meaningful and reliable simulations: schemes depending on few parameters, easily estimable through simple experiments, support quick predictions of efficient milling conditions for a given material, thus reducing and steering the experimental effort in fine-tuning the ball milling process.

As a further development, images of the milling process are going to be recorded through an high-speed camera directly mounted on the jar, therefore allowing more precise coefficients (and complicated contact models) to be retrieved via direct match of simulated and experimental trajectories. Moreover, guided by simulation outputs, molecular dynamics calculations are currently running aimed at understanding defect formation from an atomistic point of view. Finally, the power of simulations will be exploited to design more efficient jars.

Acknowledgements

The present work was partly supported by Fondazione Caritro, under project No 2013-0247 “Mechanical activation to improve bioavailability and reduce adverse effects of drugs in the therapy of chronic diseases” The authors are especially gratefulto Ing. D. Catelani (MSC Software) and Prof. S. Siboni for precious collaboration and support to the research work. N.M.P. is supported by the European Research Council (ERC StG Ideas 2011 BIHSNAM no.279985 on “Bio-inspired hierarchical supernanomaterials”, ERC PoC 2013-1 REPLICA2 no. 619448 on “Large-area replication of biological antiadhesivenanosurfaces”, ERCPoC2013-2KNOTOUGHno.632277on “Super-tough knotted fibres”), by the European Commission under the Graphene Flagship (WP10 “Nanocomposites”, no. 604391) and by the Provincia Autonoma di Trento (“Graphene nanocomposites”, no. S116/2012-242637 and reg. delib. no. 2266).

References

[1] M. Abdellaoui, E. Gaffet, The physics of mechanical alloying in a planetary ball mill: mathematical treatment, Acta Metall. Mater. 43 (3) (1995) 1087–1098.

[2] M. Vittori Antisari, A. Montone, N. Jovic, E. Piscopiello, C. Alvani, L. Pilloni, Low energy pure shear milling: a method for the preparation of graphite nanosheets, Scr. Mater. 55 (11) (2006) 1047–1050.

[3] L. Börner, J. Eckert, Nanostructure formation and steady-state grain size of ball-milled iron powders, Mater. Sci. Eng.: A 226 (1997) 541–545 (Ninth International Conference on Rapidly Quenched and Metastable Materials).

[4] O. Boytsov, A.I. Ustinov, E. Gaffet, F. Bernard, Correlation between milling parameters and microstructure characteristics of nanocrystalline copper powder prepared via a high energy planetary ball mill, J. Alloys Compd. 432 (1–2) (2007) 103–110.

[5] N. Burgio, A. Iasonna, M. Magini, S. Martelli, F. Padella, Mechanical alloying of the Fe–Zr system. correlation between input energy and end products, Il Nuovo Cim. 13 (4) (1991) 459–476.

[6] C.F. Burmeister, A. Kwade, Process engineering with planetary ball mills, Chem. Soc. Rev. 42 (2013) 7660–7667.

[7] A. Carpinteri, N. Pugno,Are scaling laws on strength of solids related to mechanics or to geometry? Nat. Mater. 4 (6) (2005) 421–423.

[8] Y. Chen, J. Fitz Gerald, J.S. Williams, S. Bulcock, Synthesis of boron nitride nanotubes at low temperatures using reactive ball milling, Chem. Phys. Lett. 299 (3–4) (1999) 260–264.

[9] CSM Instruments-Pin-on-Disk Tribometer (TRB). http://www.csminstruments.com/en/Pin-on-Disk-Tribometer.

[10] J.F. de Carvalho, S.N. de Medeiros, M.A. Morales, A.L. Dantas, A.S. Carrio, Synthesis of magnetite nanoparticles by high energy ball milling, Appl. Surf. Sci. 275 (2013) 84–87 (NANOSMAT 2012).

[11] F.P. Di Maio, A. Di Renzo, Analytical solution for the problem of frictional-elastic collisions of spherical particles using the linear model, Chem. Eng. Sci. 59 (16) (2004) 3461–3475.

[12] M. D'Incau, M. Leoni, P. Scardi, High-energy grinding of FeMo powders, J. Mater. Res. 22 (2007) 1744–1753.

[13] S. Dubowsky, F. Freudenstein, Dynamic analysis of mechanical systems with clearances-part 1: Formation of dynamic model, J. Eng. Ind. 93 (1) (1971) 305–309.

[14] A. Esawi,K. Morsi, Dispersion of carbon nanotubes (CNTs)in aluminum powder, Composites A: Appl. Sci. Manuf. 38 (2) (2007) 646–650.

[15] Y. Fan, L. Wang, J. Li, J. Li, S. Sun, F. Chen, L. Chen, W. Jiang, Preparation and electrical properties of graphene nanosheet/Al2O3 composites, Carbon 48 (6) (2010) 1743–1749.

[16] H.J. Fecht, E. Hellstern, Z. Fu, W.L. Johnson, Nanocrystalline metals prepared by high-energy ball milling, Metall. Trans. A 21 (9) (1990) 2333–2337.

[17] Y.T. Feng, K. Han, D.R.J. Owen, Discrete element simulation of the dynamics of high energy planetary ball milling processes, Mater. Sci. Eng.: A 375 (2004) 815–819.

[18] Fritsch Vario-Planetary Mill PULVERISETTE 4. http://www.fritsch-milling.com/products/milling/planetary-mills/pulverisette-4-classic-line/description/.

[19] M. Gateshki, V. Petkov, G. Williams, S.K. Pradhan, Y. Ren, Atomic-scale structure of nanocrystalline ZrO2 prepared by high-energy ball milling, Phys. Rev. B 71 (2005) 224107–224115.

[20] G. Gilardi, I. Sharf, Literature survey of contact dynamics modelling, Mech. Mach. Theory 37 (10) (2002) 1213–1239.

[21] G. De Giudici, R. Biddau, M. Dincau, M. Leoni, P. Scardi, Dissolution of nanocrystalline fluorite powders: an investigation by XRD and solution chemistry, Geochim. Cosmochim. Acta 69 (16) (2005) 4073–4083.

[22] W. Goldsmith, Impact: The Theory and Physical Behaviour of Colliding Solids, Dover Publications, 2001.

[23] E.O. Hall, The deformation and ageing of mild steel: III discussion of results, Proc. Phys. Soc. Sect. B 64 (9) (1951) 747–753.

[24] P. Heitjans, S. Indris, Fast diffusion in nanocrystalline ceramics prepared by ball milling, J. Mater. Sci. 39 (16–17) (2004) 5091–5096.

[25] E. Hellstern, H.J. Fecht, Z. Fu,W.L. Johnson, Structural and thermodynamic properties of heavily mechanically deformed Ru andAlRu, J.Appl. Phys. 65 (1)(1989) 305–310.

[26] H.M. Hilber, T.J.R. Hughes, R.L. Taylor, Improved numerical dissipation for time integration algorithms in structural dynamics, Earthq. Eng. Struct. Dyn. 5 (3) (1977) 283–292.

[27] J.Y. Huang, Y.K. Wu, H.Q. Ye, Ball milling of ductile metals, Mater. Sci. Eng.: A 199 (2) (1995) 165–172.

[28] M. Hussain, Y. Oku,A. Nakahira,K. Niihara, Effects of wet ball-milling on particle dispersion and mechanical properties of particulate epoxy composites, Mater. Lett. 26 (3) (1996) 177–184.

[29] S. Indris, D. Bork, P. Heitjans, Nanocrystalline oxide ceramics prepared by highenergy ball milling, J. Mater. Synth. Process. 8 (3–4) (2000) 245–250.

[30] T. Inoue, K. Okaya, Grinding mechanism of centrifugal mills a simulation study based on the discrete element method, Int. J. Miner. Process. 44 (1996) 425–435 (Comminution).

[31] I.-Y. Jeon, H.-J. Choi, S.-M. Jung, J.-M. Seo, M.-J. Kim, L. Dai, J.-B. Baek, Largescale production of edge-selectively functionalized graphene nanoplatelets via ball milling and their use as metal-free electrocatalysts for oxygen reduction reaction, J. Am. Chem. Soc. 135 (4) (2013) 1386–1393.

[32] J. Kano, H. Mio, F. Saito, Correlation of size reduction rate of inorganic materials with impact energy of balls in planetary ball milling, J. Chem. Eng. Jpn. 32 (4) (1999) 445–448.

[33] J. Kano, F. Saito, Correlation of powder characteristics of talc during planetary ball milling with the impact energy of the balls simulated by the particle element method, Powder Technol. 98 (2) (1998) 166–170.

[34] L.B. Kong, J. Ma, H. Huang, MgAl2O4 spinel phase derived from oxide mixture activated by a high-energy ball milling process, Mater. Lett. 56 (3) (2002) 238–243.

[35] L.B. Kong, W. Zhu, O.K. Tan, Preparation and characterization of Pb(Zr0.52Ti0.48)O3 ceramics from high-energy ball milling powders, Mater. Lett. 42 (4) (2000) 232–239.

[36] K. Kouroupis-Agalou, A. Liscio, E. Treossi, L. Ortolani, V. Morandi, N.M. Pugno, P. Vincenzo, Fragmentation and exfoliation of 2-dimensional materials: a statistical approach, Nanoscale 6 (2014) 5926–5933.

[37] H.M. Lankarani, P.E. Nikravesh, Continuous contact force models for impact analysis in multibody systems, Nonlinear Dyn. 5 (2) (1994) 193–207.

[38] L.H. Li, Y. Chen, G. Behan, H. Zhang, M. Petravic, A.M. Glushenkov, Large-scale mechanical peeling of boron nitride nanosheets by low-energy ball milling, J. Mater. Chem. 21 (2011) 11862–11866.

[39] P. Liu, X. Rong, J. Laru, B. van Veen, J. Kiesvaara, J. Hirvonen, T. Laaksonen, L. Peltonen, Nanosuspensions of poorly soluble drugs: preparation and development by wet milling, Int. J. Pharm. 411 (1–2) (2011) 215–222.

[40] H.-j. Lu, G.-Z. Liang, X.-y. Ma, B.-y. Zhang, X.-b. Chen, Epoxy/clay nanocomposites: further exfoliation of newly modified clay induced by shearing force of ball milling, Polym. Int. 53 (10) (2004) 1545–1553.

[41] H. Mio, J. Kano, F. Saito, K. Kaneko, Effects of rotational direction and rotationto-revolution speed ratio in planetary ball milling, Mater. Sci. Eng.: A 332 (1–2) (2002) 75–80.

[42] H. Mio, J. Kano, F. Saito, K. Kaneko, Optimum revolution and rotational directions and their speeds in planetary ball milling, Int. J. Miner. Process. 74 (2004) S85–S92 (Special Issue Supplement Comminution 2002).

[43] B.K. Mishra, C.V.R. Murty, On the determination of contact parameters for realistic {DEM} simulations of ball mills, Powder Technol. 115 (3) (2001) 290–297.

[44] B.K. Mishra, R.K. Rajamani, The discrete element method for the simulation of ball mills, Appl. Math. Modell. 16 (11) (1992) 598–604.

[45] MSC Adams. http://www.mscsoftware.com/it/product/adams.

[46] D. Negrut, R. Rampalli, G. Ottarsson, A. Sajdak, On an implementation of the Hilber–Hughes–Taylor method in the context of index 3 differential-algebraic equations of multibody dynamics (detc2005-85096), J. Comput. Nonlinear Dyn. 2 (1) (2006) 73–85.

[47] E.L. Parrott, Milling of pharmaceutical solids, J. Pharm. Sci. 63 (6) (1974) 813–829.

[48] J.E. Patterson, M.B. James, A.H. Forster, R.W. Lancaster, J.M. Butler, T. Rades, Preparation of glass solutions of three poorly water soluble drugs by spray drying melt extrusion and ball milling, Int. J. Pharm. 336 (1) (2007) 22–34.

[49] N.J. Petch, The cleavage strength of polycrystals, J. Iron Steel Inst. 174 (1953) 25–28.

[50] P. Pochet, E. Tominez, L. Chaffron, G. Martin, Order–disorder transformation in Fe–Al under ball milling, Phys. Rev. B 52 (1995) 4006–4016.

[51] J. Raasch, Trajectories and impact velocities of grinding bodies in planetary ball mills, Chem. Eng. Technol. 15 (4) (1992) 245–253.

[52] Á. Révész, T. Ungár, A. Borbély, J. Lendvai, Dislocations and grain size in ballmilled iron powder, Nanostruct. Mater. 7 (7) (1996) 779–788.

[53] S. Rosenkranz, S. Breitung-Faes, A. Kwade, Experimental investigations and modelling of the ball motion in planetary ball mills, Powder Technol. 212 (1) (2011) 224–230.

[54] N. Rubio, C. Fabbro, M. Antonia Herrero, A. de la Hoz, M. Meneghetti, J.L.G. Fierro, M. Prato, E. Vzquez, Ball-milling modification of single-walled carbon nanotubes: purification cutting and functionalization, Small 7 (5) (2011) 665–674.

[55] P. Scardi, M. Leoni, Whole powder pattern modelling, Acta Crystallogr. Sect. A 58 (2) (2002) 190–200.

[56] Paolo Scardi,Microstructural properties:lattice defects and domain size effects, in: R.E. Dinnebier, S.J.L. Billinge (Eds.), Powder Diffraction. Theory and Practice, RSC Publishing, Cambridge, 2008, pp. 378–416 (chapter 13).

[57] P. Scardi, M. Leoni, Diffraction line profiles from polydisperse crystalline systems, Acta Crystallogr. Sect. A 57 (5) (2001) 604–613.

[58] V. Sepelák, ˇ S. Bégin-Colin, G. Le Caër, Transformations in oxides induced by high-energy ball-milling, Dalton Trans. 41 (2012) 11927–11948.

[59] S. Sheibani, A. Ataie, S. Heshmati-Manesh, G.R. Khayati, Structural evolution in nano-crystalline Cu synthesized by high energy ball milling, Mater. Lett. 61 (14–15) (2007) 3204–3207.

[60] C.C. Silva, M.P.F. Graa, M.A. Valente, A.S.B. Sombra, Crystallite size study of nanocrystalline hydroxyapatite and ceramic system with titanium oxide obtained by dry ball milling, J. Mater. Sci. 42 (11) (2007) 3851–3855.

[61] A. Stolle, T. Szuppa, S.E.S. Leonhardt, B. Ondruschka, Ball milling in organic synthesis: solutions and challenges, Chem. Soc. Rev. 40 (2011) 2317–2329.

[62] C. Suryanarayana, Mechanical alloying and milling, Prog. Mater. Sci. 46 (1–2) (2001) 1–184.

[63] G.I. Taylor, The mechanism of plastic deformation of crystals. PartI. Theoretical, Proc. R. Soc. Lond. A: Math. Phys. Eng. Sci. 145 (855) (1934) 362–387.

[64] S. Vives, E. Gaffet, C. Meunier, X-ray diffraction line profile analysis of iron ball milled powders, Mater. Sci. Eng.: A 366 (2) (2004) 229–238.

[65] VV.AA, Defect and Microstructure Analysis by Diffraction, Oxford University Press, 1999.

[66] VV.AA, Diffraction Analysis of the Microstructure of Materials, Springer, 2004.

[67] VV.AA, High-Energy Ball Milling: Mechanochemical Processing of Nanopowders, Woodhead Publishing, 2010.

[68] T.P. Yadav, O.N. Srivastava, Synthesis of nanocrystalline cerium oxide by high energy ball milling, Ceram. Int. 38 (7) (2012) 5783–5789.

[69] M. Zakeri, M.R. Rahimipour, B. Jamal Abbasi, Synthesis of nanostructure tetragonal ZrO2 by high energy ball milling, Mater. Technol. 28 (4) (2013) 181–186.

[70] M. Zakeri, M. Razavi, M.R. Rahimipour, B. Jamal Abbasi, Effect of ball to powder ratio on the ZrO2 phase transformations during milling, Physica B: Condens. Matter 444 (2014) 49–53.

[71] W. Zhao, F.Wu, H.Wu, G. Chen, Preparation of colloidal dispersions of graphene sheets in organic solvents by using ball milling, J. Nanomater. 2010 (2010) 6:1–6:4.

Table 1
Geometrical and physical properties of jar and milling media for the presented case study.

Jar (AISI 304)	
Radius	32.5 mm
Volume	80 cm^3
Density	8.03 g/cm^3
Young modulus	193 GPa
Poisson ratio	0.29

Spheres (AISI C1020)	
Number	12
Radius	6 mm
Density	7.85 g/cm^3
Young modulus	200 GPa
Poisson ratio	0.29

Table 2
Values used for the contact model and method applied for their derivation.

Sphere–sphere generalized contact stiffness, k_{ss}	252,146 $N/mm^{3/2}$	Eq. (3)
Sphere–plane generalized contact stiffness, k_{sp}	350,236 $N/mm^{3/2}$	Eq. (4)
Restitution coefficient, e	0.516	Drop test, $e = \sqrt{h/h_0}$
Relative impact velocity, $\dot{u}_{n0}$	3,309 mm/s	Statistical analysis of velocities
Sphere–sphere contact damping, $c_{m,ss}$	10.1 kg/s	Eq. (5)
Sphere–plane contact damping, $c_{m,sp}$	17.5 kg/s	Eq. (5)
Full damping penetration depth, d	0.211 mm	Fit of experimental drop test results

Table 3
Friction coefficients, stiction (v_s) and friction (v_d) transition velocities used in the simulation. Pin-on-disc tests were performed using CSM tribometer [9].

	Steel–steel	Steel–fluorite	
μ_s	1.0	0.25	Literature
μ_d	0.8	0.2	Tribological test
v_s	1 mm/s	1 mm/s	Statistical analysis of velocities
v_d	10 mm/s	10 mm/s	Statistical analysis of velocities

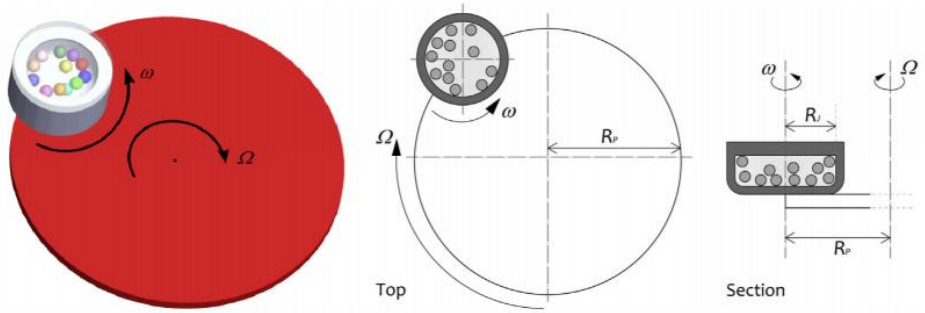

Fig. 1. Schematic representation of a planetary ball-mill. Left, three-dimensional view; middle and right, definition of the jar radius R_j and the distance between axis of rotation (angular velocity ω) and revolution (angular velocity Ω) R_p.

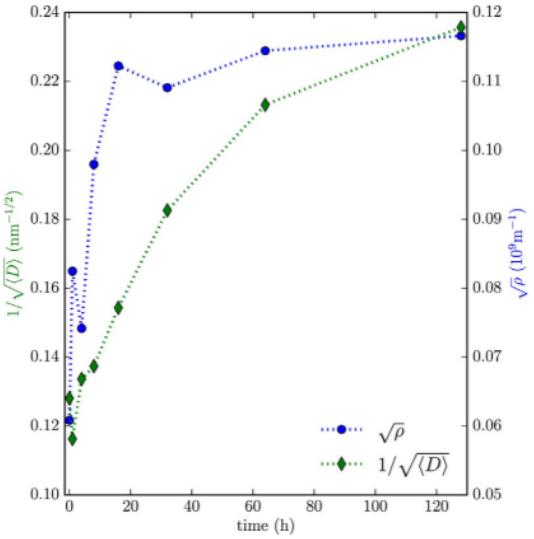

Fig. 2. Average crystallite size ($\langle D\rangle$) and dislocation density (ρ) as a function of the milling time presented from the point of view of the Hall–Petch law (yield stress) and Taylor equation (work hardening) [21].

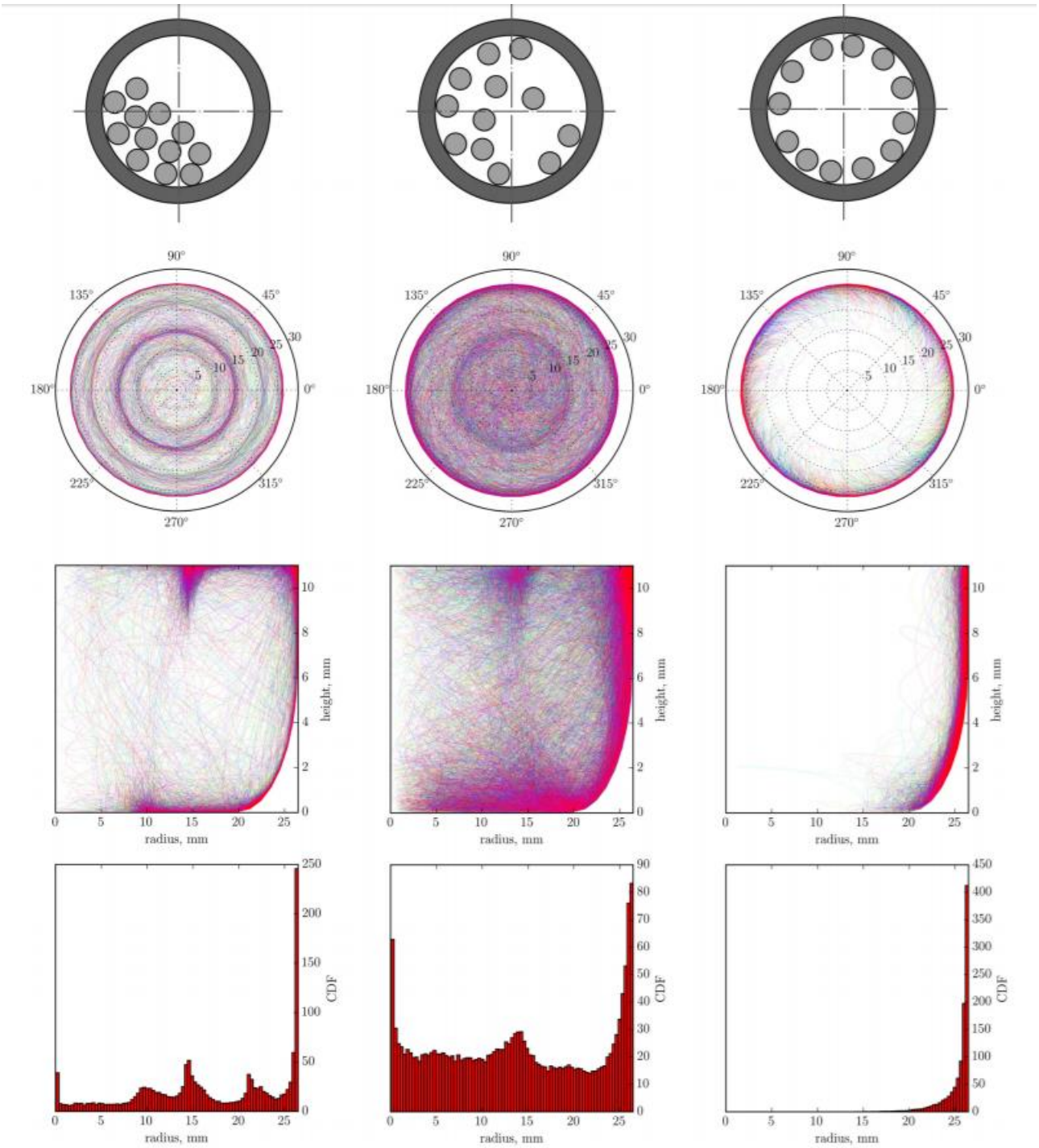

Fig. 3. Top row, scheme of typical motion regime, from left to right (i) cascading, (ii) cataracting and (iii) rolling. Second and third row, trajectories (lines) within the jar ($\omega = -320, -600, -800$ rpm and $\Omega = 200$ rpm), polar coordinates (top) top view and (bottom) section. Bottom row, CDF (Eq. (9)). Left to middle, the uniformity of the histograms increases (random motion); middle to right, balls tend to stick to the jar surfaces.

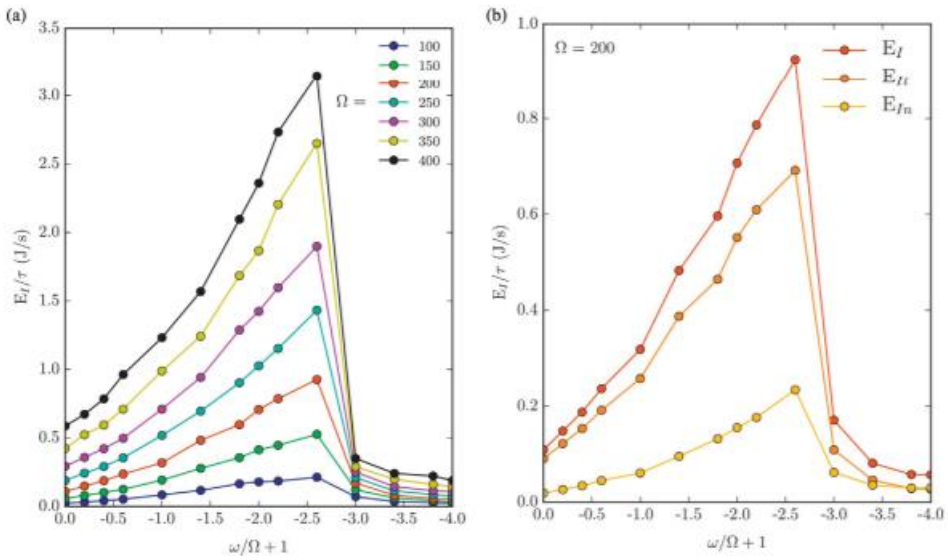

Fig. 4. Specific impact energy for the steel–steel case as a function of the jar to plate angular velocities. Left: effect of incrementing the plate velocity Ω: while the energy increases, interestingly the location of its maximum is approximately not changing. Right: the specific energy of the curve with Ω = 200 rpm is broken down into its normal (E_{In}) and tangential (E_{It}) components (with respect to the local impact reference frame).

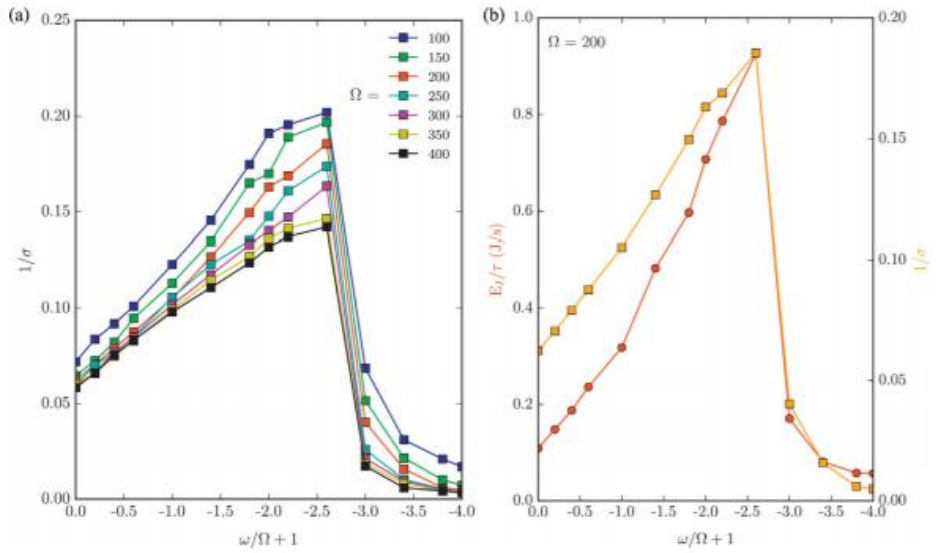

Fig. 5. Left: geometrical parameter for the steel–steel case as a function of the jar to plate angular velocities. Right: comparison of the geometrical parameter and the specific impact energy for the simulation with Ω = 200 rpm: the behavior is approximately the same.

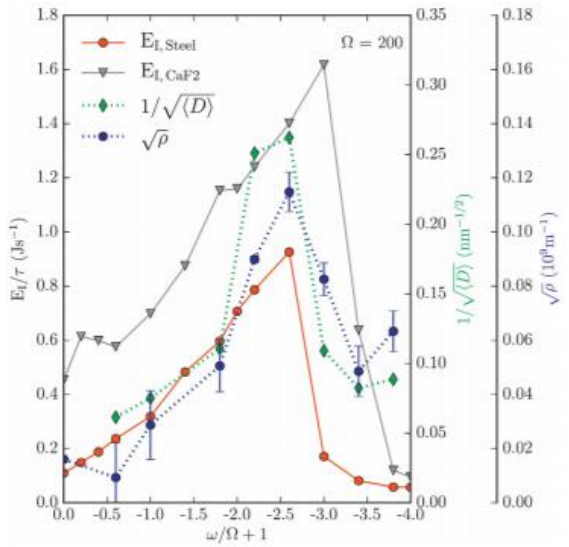

Fig. 6. Specific impact energy for Ω = 200 rpm and both steel–steel (red) and steel–fluorite (gray) interaction coefficients. LPA from XRPD data of ball milled calcium fluoride are also reported. Particularly, the reciprocal square root of the average crystallite size (green) and the square root of the dislocation density (blue), respectively, proportional to the Hall–Petch and Taylor trends. (For interpretation of the references to color in this figure legend, the reader is referred to the web version of this article.)